Combined Pressure and Diffusional Transition Region Flow of Gases in Porous Media

AYAD A. ALZAYDI
University of Riyadh,
Riyadh, Saudi Arabia

CHARLES A. MOORE
and
IQBAL S. RAI
The Ohio State University
Columbus, Ohio

Expressions were derived for combined pressure and diffusional transition region flow of gases in porous media. Experimental systems were developed to verify the applicability of the equations for packed columns of Kaolinite clay and quartz sand with methane and carbon dioxide flowing into nitrogen.

SCOPE

The prediction of flow behavior of mixed gases in porous media under small pressure gradients is important in manufacturing processes and in transport processes in soils. The motivation for the present research was the necessity to predict migration patterns of methane and carbon dioxide in soils around sanitary landfills.

The flow processes involved are very complex. The problem would be simpler if the flow process were purely diffusional or purely pressure flow. However, gas generated in landfills exhibits high concentrations and total pressures just greater than atmospheric. Thus, small total pressure gradients and high partial pressure gradients exist. The use of the term combined flow implies that diffusional and pressure flow become competitive, and neither can be ignored.

The pore sizes encountered in soils (and many packed beds) are of just such a size that gas flow at atmospheric pressure is accompanied by molecule to molecule as well as molecule to soil collisions. Thus, both Knudsen diffusion and bulk diffusion are involved in the flow process, as implied in the use of the term transition region flow.

CONCLUSIONS AND SIGNIFICANCE

It was concluded from the study that the mathematical expressions derived to describe the flow process gave reasonable predictions of gas concentration as a function of time. Moreover, examination of the results of the analytical predictions verified that the experimental system met the criteria for combined transition region flow.

The conclusions are significant in that they show that physical/mathematical models that have been developed for simple flow conditions can be combined to predict flow in the much more complicated systems that are encountered in practical applications.

Excellent reviews of the large body of literature devoted to developing expressions for the transport of gases in porous media have been presented by Youngquist (1970), Gunn and King (1969), and Satterfield and Cadle (1968), among others.

The central issue which is currently being addressed by researchers, not only in flow of gases in porous media but in all disciplines involving multicomponent systems, is the degree to which the experimentally determined parameters can be decoupled. In a fully decoupled approach, certain parameters unique to each gas and others unique to the porous medium must be experimentally determined; however, there is no necessity to determine experimental parameters unique to the particular gas-porous medium combination.

Various arguments may be presented for the degree to which a given problem should be decoupled. If a narrow range of alternative solutions to a particular application is sought, it may be easier to perform experiments to determine one or two coupled parameters than to perform experiments to obtain decoupled parameters. Furthermore, such experiments not only provide data for determining the required parameters but also offer confirmation (in a somewhat self-serving manner) of the applicability of the theory to the particular system of interest. A disadvantage of this approach is that the data obtained are valid only for the particular system studied.

A fully decoupled approach is preferred if a wide range of systems is being studied or if a high degree of optimization of system variables is to be undertaken.

The following observations can be made with respect to the present state-of-the-art for flow of gases in a generalized porous medium:

1. Analytical expressions have been derived for isobaric multicomponent diffusional flow and for single-component pressure flow. Only decoupled experimental parameters are required.

2. Rational expressions have been developed for combined pressure and diffusional flow. However, it is not clear whether decoupled transport coefficients can be obtained.

The objective of this paper is to present the experimental verification of a rational, fully decoupled expres-

0001-1541/78/9667-0035/$01.15

sion for combined pressure and diffusional transition region flow of gases in porous media. This objective is met by deriving analytical expressions for the process, by presenting experimental results, by analytically predicting the experimental results using decoupled parameters, and by discussing the degree to which the theory is substantiated by the experiments and the degree to which the experimental systems employed met the criteria for combined transition region flow.

THEORY

Diffusional Flow in a Capillary Tube

As a gas flows isobarically in a capillary tube, its progress is impeded by collisions with other gas molecules and with the capillary walls. If only collisions with the walls (Knudsen diffusion) are involved, the molecules behave independently of each other, and the diffusion equation for component i is given by Knudsen (1909) as

$$\frac{1}{RT} N_{Ki}^{D} = D_{Ki} \frac{\partial p_i}{\partial z} \tag{1}$$

where

$$D_{Ki} = 9.7 \times 10^{-5} \cdot r \frac{T}{M_i} = K_i \cdot r \tag{2}$$

If only collisions with other molecules (bulk diffusion) occur, then the collisions may be between like or unlike species of gas, and the diffusion equation for a multicomponent gas is given by

$$-\frac{1}{RT}\frac{\partial p_i}{\partial z} = \sum_{\substack{j=1 \\ j \neq i}}^{n} \frac{N_i^D x_j - N_j^D x_i}{D_{ij}^o} \tag{3}$$

When both wall and intermolecular collisions occur (transition region diffusion), Rothfeld (1963) and Scott and Dullien (1962) used a flux momentum balance in an open system and expressed the diffusion by

$$\frac{1}{RT}\frac{\partial p_i}{\partial z} = \frac{N_i^D}{D_{Ki}} + \sum_{\substack{j=1 \\ j \neq i}}^{n} \frac{N_i^D x_j - N_j^D x_i}{D_{ij}^o} \tag{4}$$

Equation (4) can be solved for N_i to give

$$N_i^D = -\left[\frac{1}{K_i \cdot r} + \sum_{\substack{j=1 \\ j \neq i}}^{n} \left[\frac{x_j - x_i \dfrac{N_j^D}{N_i^D}}{D_{ij}^o} \right] \right]^{-1} \cdot \frac{1}{RT} \cdot \frac{\partial p_i}{\partial z} \tag{5}$$

Remick and Geankoplis (1973) treated this case for binary gases.

Pressure Flow in a Capillary Tube

If a total pressure gradient exists in a capillary tube, transport will occur by Poiseuille flow and by slip flow along the capillary walls. This type of flow may be treated analogously to flow of compressible fluids in tubes. Scott and Dullien (1962) used modern kinetic theory to derive the following expression for multicomponent gases:

$$F = -\left[\frac{r^2}{8\mu_{\text{mix}}} + \frac{r}{S_{\text{mix}}} \right] \cdot \frac{P}{RT} \cdot \frac{\partial P}{\partial z} \tag{6}$$

The viscosity of the mixture is given by Wilke (1950) and Buddenburg and Wilke (1949) as

$$\mu_{\text{mix}} = \sum_{i=1}^{n} \frac{x_i \mu_i}{\sum_{j=1}^{n} x_j \Phi_{ij}} \tag{7}$$

in which

$$\Phi_{ij} = \frac{1}{\sqrt{8}} \left(1 + \frac{M_i}{M_j} \right)^{-1/2} \left[1 + \left(\frac{\mu_i}{\mu_j} \right)^{1/2} \left(\frac{M_j}{M_i} \right)^{1/4} \right]^2 \tag{8}$$

and

$$S_{\text{mix}} = \frac{3 \sum_{i=1}^{n} M_i \bar{v}_i p_i}{4RT} \tag{9}$$

The mean molecular velocity $\bar{v}_i$ is given by

$$\bar{v}_i = \left(\frac{8RT}{\pi M_i} \right)^{1/2} \tag{10}$$

Substituting (10) into (9), we get

$$S_{\text{mix}} = 3 \sum_{i=1}^{n} \left(\frac{M_i}{2\pi RT} \right)^{1/2} p_i \tag{11}$$

Combined Pressure and Diffusional Flow in a Capillary Tube

If both partial and total pressure gradients are present, a combination of diffusional and pressure flows will occur. Evans, Watson, and Mason (1962) have shown that the combined flow may be given by the sum of the individual contributions from diffusion and pressure flow, provided that the pressure dependancy of D_{ij} is taken into consideration. For component i, the combined flow is

$$N_i^T = N_i^D + x_i F = N_i^D + N_i^P \tag{12}$$

Substituting Equations (5) and (6) into (12), we get

$$N_i^T = -\left[\frac{1}{K_i r} + \sum_{j=1}^{n} \left[\frac{x_j - x_i \dfrac{N_j^D}{N_i^D}}{D_{ij}^o} \right] \right]^{-1} \frac{1}{RT} \frac{\partial p_i}{\partial z} - \left[\frac{r^2}{8\mu_{\text{mix}}} + \frac{r}{S_{\text{mix}}} \right] \frac{p_i}{RT} \frac{\partial P}{\partial z} \tag{13}$$

Generalization to a Porous Medium

The equations derived above all apply to flow in a capillary tube of radius r. In generalizing to a porous medium, it is necessary to account for the reduced flow area due to the solid phase, the variety of pore sizes which may be present, and the probable circuitous path followed by a given gas molecule in traversing the medium. The parallel pore model has been used with some success and is relatively easy to apply. The approach is predicated upon representing the porous medium as an aggregation of parallel tubes, each of constant radius, which simulate the pore size distribution of the medium as determined by mercury porosimetry and/or nitrogen adsorption. The sum of the volume fractions of each pore size equals the macroscopic porosity of the medium. While the determination of the pore size distribution may be tedious, the conceptual level of detail corresponds to that involved in obtaining the required decoupled gas parameters employed in the previous sections.

The circuitousness of travel of a given molecule is usually accounted for by a tortuosity factor. While this factor has been approached analytically by Wheeler (1955) and Petersen (1958), it is also frequently used by researchers as a parameter which is adjusted to

achieve agreement with experimental data (fudge factor approach). Alzaydi (1975) has organized data from the literature which show that such experimentally determined tortuosities increase with decreasing mean pore size. This suggests that tortuosity might best be taken as a function of pore radius. If we take this approach, Equation (13) can be generalized for porous media as

$$N_i^T = -\frac{1}{RT}\sum_{r_{min}}^{r_{max}}\frac{f_v(r)}{\tau(r)}\left\{\left[\frac{1}{K_i r} + \sum_{j=1}^{n}\left[\frac{x_j - x_i\frac{N_j^D}{N_i^D}}{D_{ij}^o}\right]\right]^{-1}\frac{\partial p_i}{\partial z} + \left[\frac{r^2}{8\mu_{mix}} + \frac{r}{S_{mix}}\right]p_i\frac{\partial P}{\partial z}\right\} \quad (14)$$

The function $\tau(r)$ can either be taken as a constant (as it will be for the present work), or it could be empirically determined by fitting a curve through accumulated data as proposed by Alzaydi (1975).

The fluxes must be determined within the constraints of conservation of matter for each component:

$$\frac{1}{RT}\frac{\partial p_i}{\partial t} = -\frac{\partial N_i^T}{\partial z} \quad (15)$$

Equations (14) and (15) constitute a system of simultaneous highly nonlinear parabolic partial differential equations. Rai and Moore (1977) have discussed numerical solutions for the general multicomponent and multidimensional case. However, for the present work experimental verification is limited to binary systems in one dimension.

For such systems, Equation (14) becomes

$$N_A^T = -\frac{1}{RT}\sum_{r_{min}}^{r_{max}}\frac{f_v(r)}{\tau}\left[\left(\frac{D_{AB}^o D_{KA}}{D_{AB}^o + P_A D_{KB} + P_B D_{KA}}\right)\frac{\partial p_A}{\partial z} + \left(\frac{D_{KA}D_{KB}}{p_A D_{KB} + p_B D_{KA} + D_{AB}^o} + \frac{r^2}{8\mu_{AB}} + \frac{r}{S_{mix}}\right)p_A\frac{\partial P}{\partial z}\right] \quad (16a)$$

and Equation (13) becomes

$$\frac{1}{RT}\frac{\partial p_A}{\partial t} = -\frac{\partial N_A^T}{\partial z} \quad (17a)$$

Analogous expressions for component B will not be written but will be subsequently referred to as Equations (16b) and (17b).

Solution of the Binary Transport Equations

Eqs. (16) and (17) can be written in more concise notation:

$$N_A^T = -\frac{1}{RT}(D_A\nabla p_A + D_{psA}\nabla P) \quad (18a)$$

$$N_B^T = -\frac{1}{RT}(D_B\nabla p_B + D_{psB}\nabla P) \quad (18b)$$

$$\frac{1}{RT}\dot{p}_A = -\nabla N_A^T \quad (19a)$$

$$\frac{1}{RT}\dot{p}_B = -\nabla N_B^T \quad (19b)$$

where

$$D_A = \sum_{r_{min}}^{r_{max}}\frac{f_v(r)}{\tau}\left(\frac{D_{AB}^o D_{KA}}{D_{AB}^o + p_A D_{KB} + p_B D_{KA}}\right) \quad (20)$$

$$D_{psA} \equiv \sum_{r_{min}}^{r_{max}}\frac{f_v(r)}{\tau}\left(\frac{D_{KA}D_{KB}}{p_A D_{KB} + p_B D_{KA} + D_{AB}^o} + \frac{r^2}{8\mu_{AB}} + \frac{r}{S_{mix}}\right)p_a \quad (21)$$

and similarly for component B.

The solution is facilitated by rearranging Equations (19):

$$N_A^T = -\frac{1}{RT}[(D_A + D_{psA})\nabla p_A + (D_{psA})\nabla p_B] \quad (22a)$$

$$N_B^T = -\frac{1}{RT}[(D_B + D_{psB})\nabla p_B + (D_{psB})\nabla p_A] \quad (22b)$$

Equations (22) were solved using a finite-difference predictor-corrector technique:

1. Predictor step. An explicit algorithm is used to solve for p_A and p_B at the midtime interval. These values are used to compute D_A, D_B, D_{psA}, and D_{psB}.
2. Corrector step. A Crank-Nicolson (implicit) scheme is used to compute p_A and p_B at the end of the time interval

$$\dot{p}_A = \nabla\tilde{D}_A\nabla\left(\frac{p_A^{t+\Delta t} + p_A^t}{2}\right) + \tilde{D}_{psA}\nabla\tilde{p}_B \quad (23)$$

where the tilde denotes quantities estimated from the predictor step. An analogous equation is solved for component B. This approach is accurate and stable for pressure differences of the order of 1 atm and only requires the solution of three-banded matrices.

EXPERIMENTAL VERIFICATION PROGRAM

Apparatus

Experimental apparatus shown in Figure 1 was developed to study the unsteady state combined flow of multicomponent gases in packed columns. The glass sample tube, s, consists of from one to four 0.91 m (3 ft) long sections. The tube has an inside diameter of 0.0635 m (2.5 in.). Ports t are placed on 0.152 m (6 in.) centers along the tube to allow sampling of gas and measurement of pressure.

The sampling tube is connected to a mixing chamber l which serves to mix the gases and control the inlet pressure. Chamber pressure is measured by an electrical transducer k. An electronic comparator circuit compares the actual pressure with a reference voltage representing the desired pressure and controls solenoid value i. When the solenoid valve is open, oil flows from cylinders h to cylinder j, increasing the pressure in the mixing chamber. When the reference pressure is reached, the solenoid closes. A similar system is employed at the right end of the sample tube. The detailed operating procedure is given by Alzaydi (1975).

Tests Performed

The objective of the experimental program was to obtain data for verifying equations (18) and (19) under conditions of combined transition region flow. In order to accomplish this objective, two packed powders were chosen. For uniform pores, an Ottawa sawing sand (silica) was obtained from the Ottawa silica company, Ottawa, Illinois. For distributed pore sizes, a kaolinite clay was obtained in dry powdered form from

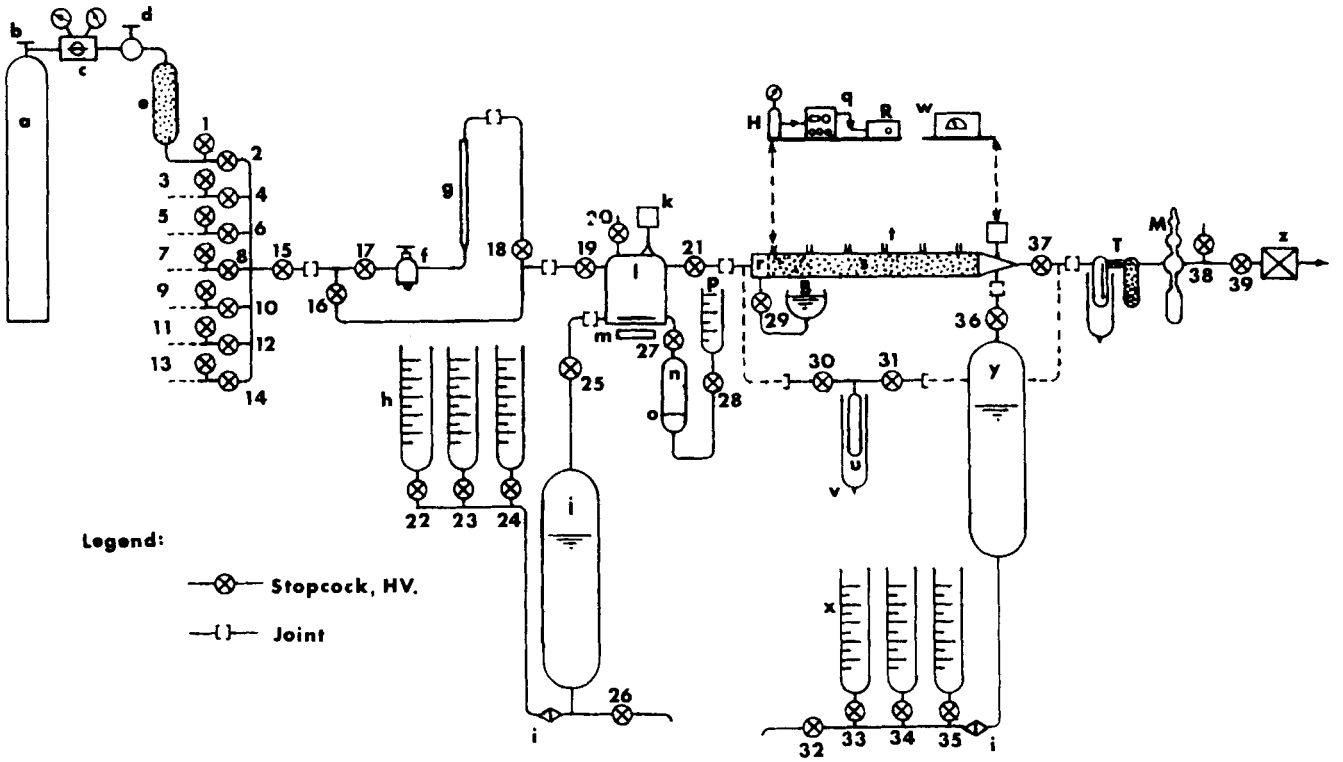

Fig. 1. Experimental apparatus.

a	=	gas cylinder
b	=	cylinder valve
c	=	pressure regulator for the gas cylinder
d	=	pressure relief valve
e	=	drying agent
f	=	pressure regulator for the high flow rate system
g	=	flowmeter
h	=	graduated cylinders
i	=	solenoid valve
j	=	storage tank
k	=	pressure transducer
l	=	mixing chamber
m	=	mixing device
n	=	volume calibration cylinder
o	=	mercury reference point
p	=	graduated cylinder
q	=	gas partitioner unit
r	=	sample reference point
s	=	soil sample tube
t	=	pressure and sampling ports
u	=	soil sample in the adsorption experiment
v	=	liquid nitrogen container
w	=	pressure transducers amplifier unit
x	=	graduated cylinders
y	=	storage tank
z	=	mechanical and diffusion pumps
B	=	mercury container
H	=	helium cylinder
R	=	recorder
M	=	McLeod gauge
T	=	trap unit

R. T. Vanderbilt Company, New York. The pore size distribution curves for these materials as packed was determined by a mercury injection method at the Gulf Research and Development Company. The results are shown in Figure 2. The pore size distribution for the Kaolinite clearly places the flow in the transition region. For the sand, bulk diffusional flow probably predominated.

In order to insure combined flow, relatively small pressure differences (1.7 $\times$ 10^3 and 3.4 $\times$ 10^3 Pa) were imposed. Combined flow was clearly present in the Kaolinite, whereas in the sand, pressure flow probably predominated. In all tests, the ambient pressure was 1.013 $\times$ 10^5 Pa. Additional data were also obtained for pure isobaric diffusional flow.

The gases employed were nitrogen, methane, carbon dioxide, oxygen, and air. The various experimental configurations employed are summarized in Table 1.

ANALYTICAL PREDICTION OF EXPERIMENTAL RESULTS

The computer code previously described was used to predict the experimental results. The input data required for the gases are summarized in Table 2.

The properties of the porous media include tortuosity and pore size distribution. For sand, τ = 1.1, and for Kaolinite, τ = 1.5. The pore size distributions as incrementally approximated based on the curves of Figure 2 are given in Table 3.

The initial pressure within the sample tube was taken as 1.013 $\times$ 10^5 Pa, and the pressure at the invading gas end was 1.013 $\times$ 10^5, 1.030 $\times$ 10^5, and 1.048 $\times$ 10^5 Pa. The temperature was 298°K. In some cases, it was found that the experimental apparatus was not capable of maintaining the desired boundary condition at the invading gas end of the sample tube. In these cases, the boundary condition at the end was varied in the computer program to match the actual measured boundary condition.

Based on these input data, the computer program predicted partial and total pressures as a function of time and position along the sample tube. In the figures to be presented subsequently, these predicted results are

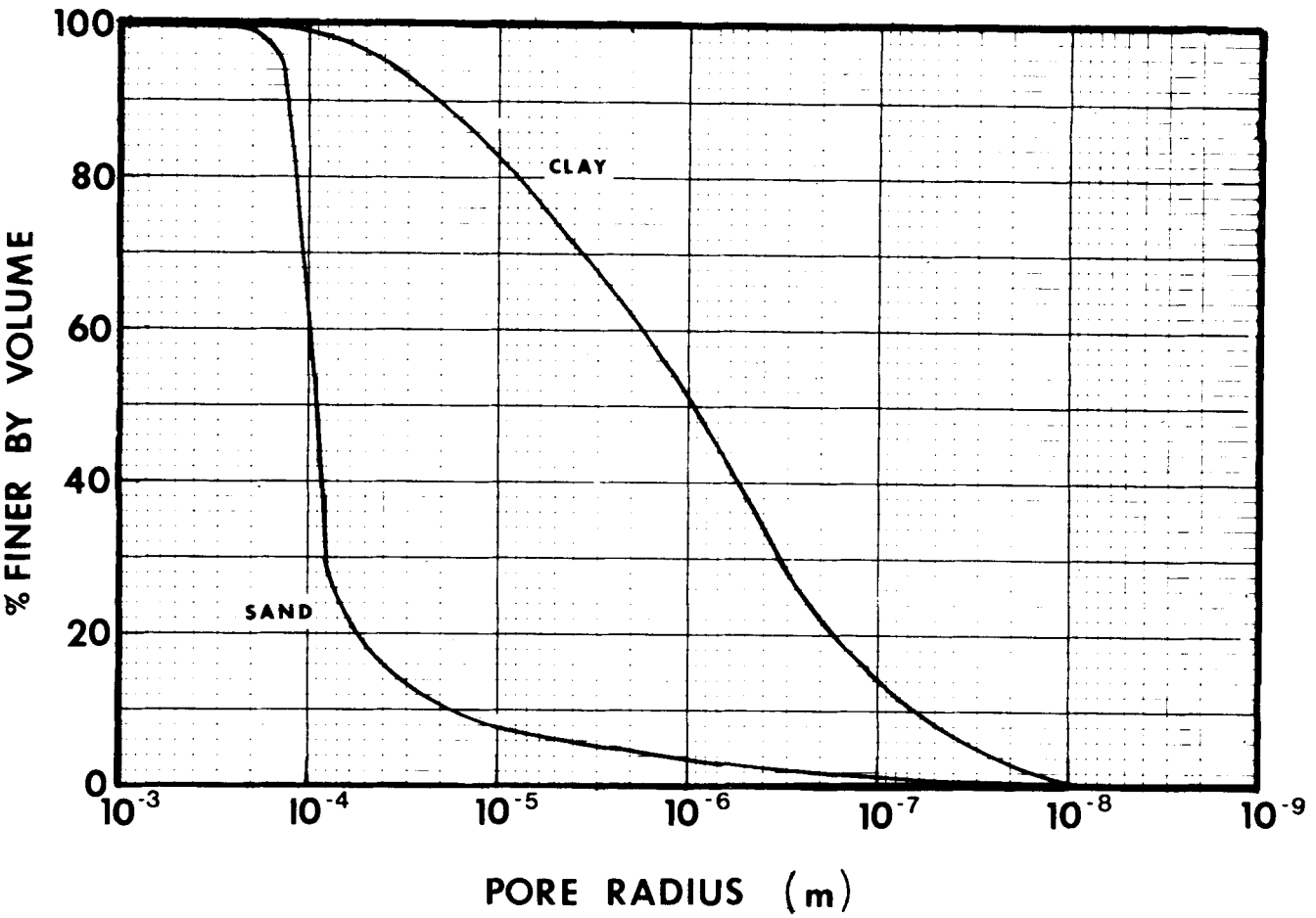

Fig. 2. Pore size distribution curves for soils used.

shown as solid lines which may be compared with the experimental data.

Comparison of Experimental and Analytical Results

Forced flow of gases in sand (air-air, nitrogen-nitrogen, oxygen-oxygen, carbon dioxide-carbon dioxide, methane-methane): In all cases, a linear total pressure gradient was achieved within 60 s. Therefore, the time dependent behavior was not observed. However, the linear pressure gradient at steady state is as predicted by the theory.

Forced flow of air in Kaolinite: As shown in Figure 3*a*, the anticipated linear pressure gradient was reached within 1,000 s. In general, the experimental data lead the theoretical predicted values slightly.

Pure diffusional flow in sand (methane into nitrogen, carbon dioxide into nitrogen): Figure 3*b* shows the pure diffusional flow for methane into nitrogen. At steady state, a concave downward profile exists because the molecular weight of methane is less than that of nitrogen. However, the degree of concavity is slightly higher in the experimental data than that predicted by theory. Figure 3*c* presents the results for carbon dioxide into nitrogen. At steady state, a concave upward profile develops because the molecular weight of carbon dioxide is higher than that of nitrogen. Again, the experimental degree of concavity is greater than that predicted theoretically.

Diffusional and combined diffusional and forced flow of methane into nitrogen in Kaolinite: Figures 4*a* through *c* present the results of a sequence of tests designed to investigate pure diffusional and combined pressure and diffusional flow of methane into nitrogen in Kaolinite. The pure diffusional flow data of Figure 4*a* show the anticipated concave downward profile. When a small total pressure gradient is introduced (Figures 4*b* and *c*), the steady state profile shows an accentuated concavity. In general, the concavity of the experimental data is somewhat less than that predicted analytically.

Diffusional and combined diffusional and forced flow of carbon dioxide into nitrogen in Kaolinite: Figures 4*d* through *f* show the results of a series of tests designed to investigate pure diffusional and combined pressure and diffusional flow of carbon dioxide into nitrogen in Kaolinite. For the purely diffusional flow (Figure 4*d*), the steady state profile shows a concavity upward as predicted by theory. However, as shown in Figures 4*e* and *f*, a small imposed total pressure gradient reverses the concavity so that both pressure flow curves are concave downward.

Assessment of the Experimental Verification of the Theory

The agreement between the experimental data and the analytical results is within the accuracy of the techniques employed. In those instances where there are noticeable discrepancies, there is no consistent trend shown. Thus, it may be concluded that the theory adequately represents the physical process manifested in the experimental conditions.

DISCUSSION

Several important aspects of the flow process were exhibited in the experiments. In order to present these aspects in the clearest manner, some purely analytical results will be examined. The purpose of this development is to present qualitatively interesting aspects of the combined pressure and diffusional flow process in the transition region and to demonstrate that the experimental systems employed yield data within this desired region.

TABLE 1. EXPERIMENTAL PROGRAM*

Invading gas	Ambient gas N_2	CH_4	CO_2	O_2	Air
N_2	1.048 (s)				
CH_4	1.013 (s, k) 1.030 (s, k) 1.048 (s, k)	1.048 (s)			
CO_2	1.013 (s, k) 1.030 (s, k) 1.048 (s, k)		1.048 (s)		
O_2				1.048 (s)	
Air					1.048 (s, k)

* Numbers denote invading gas pressure in Pascals $\times 10^{-5}$. Ambient gas pressure is 1.013×10^5 Pa. Letters denote experiments in sand (s) and Kaolinite (k).

TABLE 2. DATA FOR GASES

Parameter	Value N_2	CH_4	CO_2	O_2	Air	Joint
M_i (g/mole)	28.02	16.05	44.01	32.00		—
μ_i (Ns/m^2)	1.8×10^{-5}	1.1×10^{-5}	1.5×10^{-5}	2.0×10^{-5}	1.8×10^{-5}	—
$D_{AB}^{\circ}\left(\frac{Pa\,m^2}{s}\right)$	X		X			1.57×10^{-5}
	X	X				2.22×10^{-5}

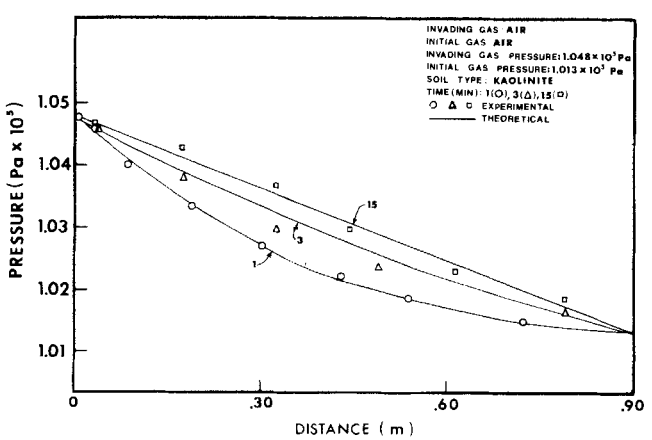

Fig. 3(a). Pressure flow of air into air in kaolinite.

TABLE 3. PORE SIZE DISTRIBUTION

	r (m)	$f_v(r)$
Kaolinite:	7×10^{-5}	0.028
	3×10^{-5}	0.056
	1×10^{-5}	0.084
	4×10^{-6}	0.084
	1.2×10^{-6}	0.084
	7×10^{-7}	0.084
	4×10^{-7}	0.084
	2.2×10^{-7}	0.084
	1.1×10^{-7}	0.056
	3×10^{-8}	0.056
		Sum = 0.70 = porosity
Sand:	4×10^{-5}	0.306
	3×10^{-6}	0.034
		Sum = 0.34 = porosity

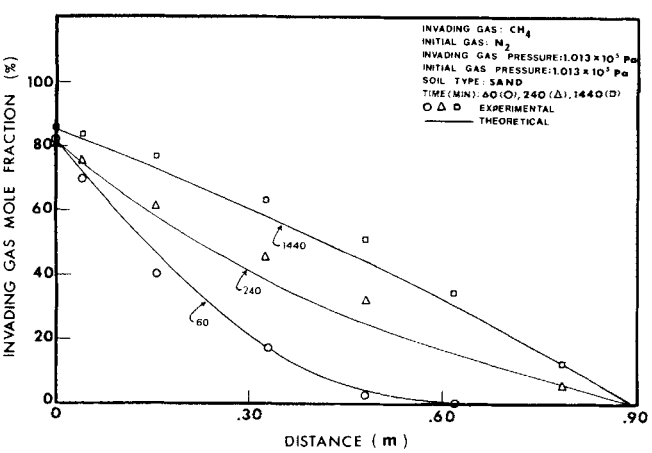

Fig. 3(b). Diffusional flow of methane into nitrogen in sand.

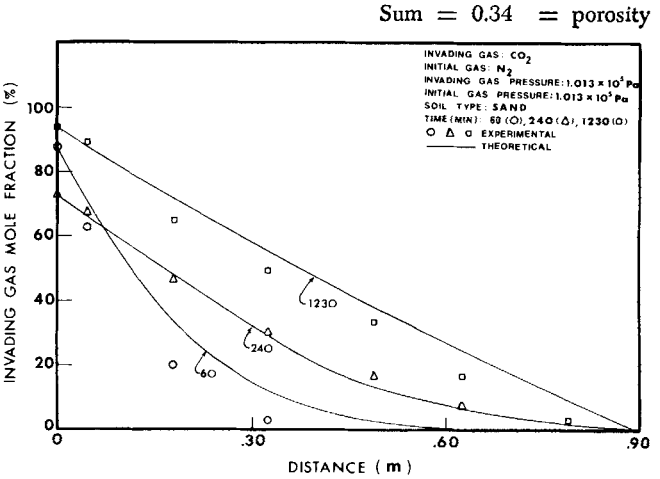

Fig. 3(c). Diffusional flow of carbon dioxide into nitrogen in sand.

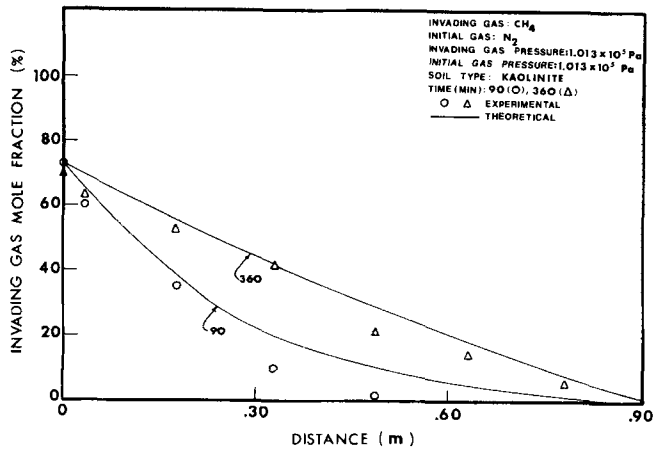

Fig. 4(a). Diffusional flow of methane into nitrogen in kaolinite.

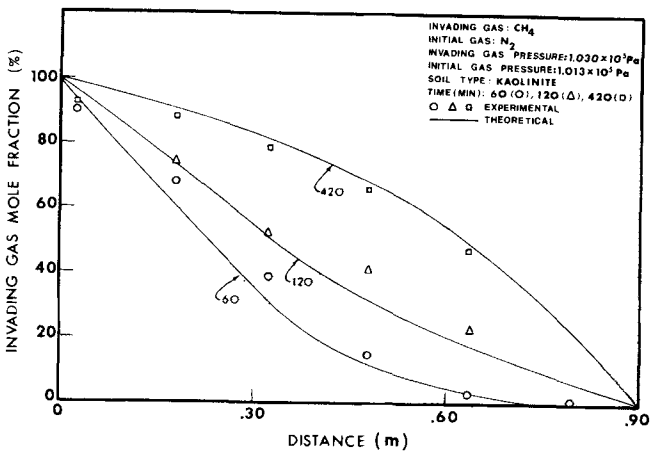

Fig. 4(b). Combined flow of methane into nitrogen in kaolinite.

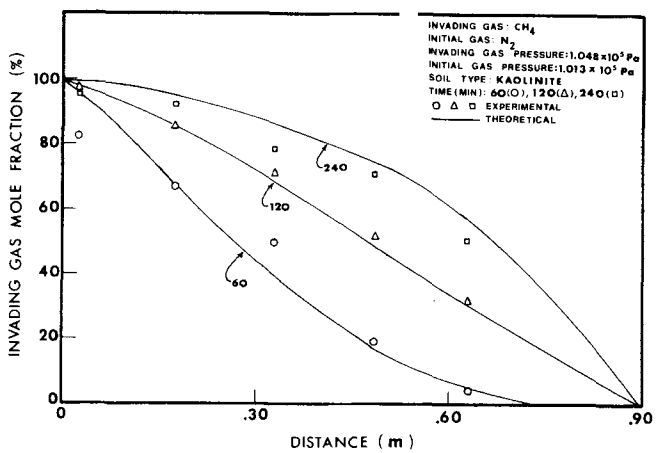

Fig. 4(c). Combined flow of methane into nitrogen in kaolinite.

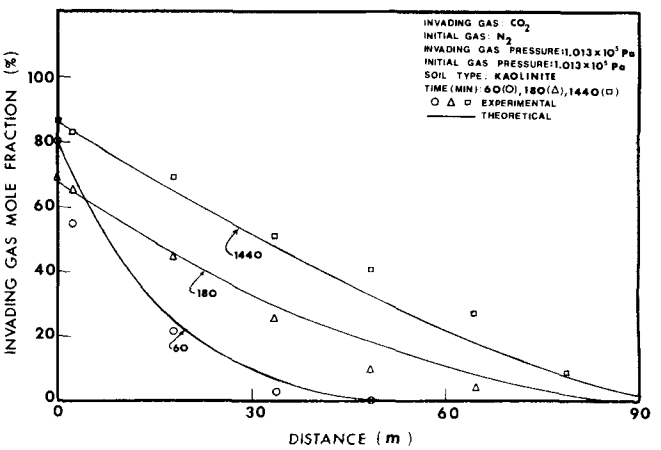

Fig. 4(d). Diffusional flow of carbon dioxide into nitrogen in kaolinite.

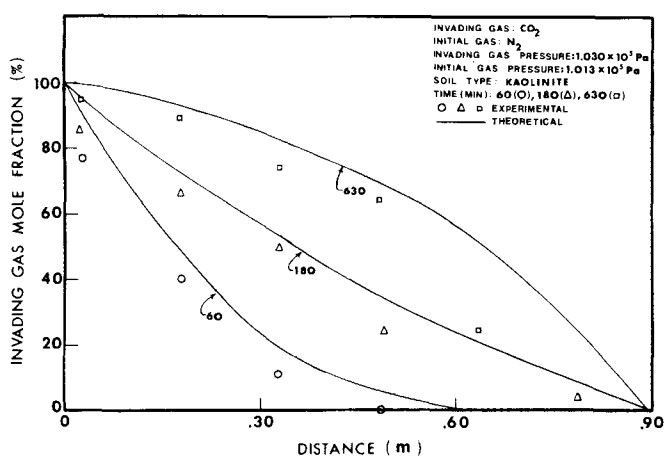

Fig. 4(e). Combined flow of carbon dioxide into nitrogen in kaolinite.

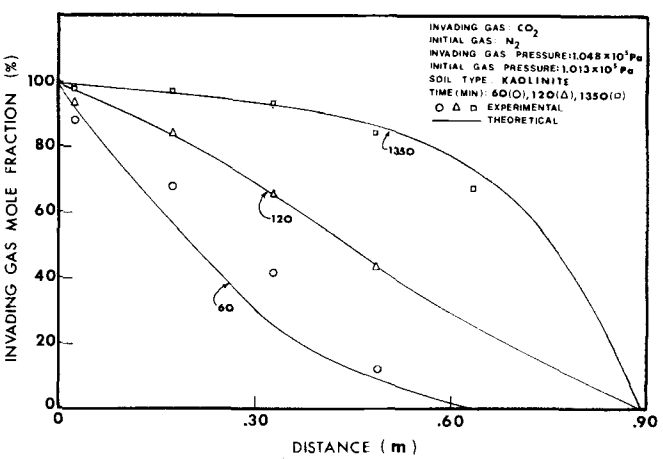

Fig. 4(f). Combined flow of carbon dioxide into nitrogen in kaolinite.

Figure 5 presents analytical results for pure diffusional flow of methane and of carbon dioxide into nitrogen in Kaolinite. The time corresponds essentially to steady state, and the curves for methane and carbon dioxide are comparable to the high time curves for Figures 3*b* and *c*, respectively. Superposition of the two curves shows that at steady state, the carbon dioxide profile is concave upward, while the methane profile is concave downward. The curvature occurs because the Knudsen diffusion coefficient as given by Equation (2) for the invading gas (methane or carbon dioxide) is different than that for the initial gas (nitrogen). This difference arises because of differences in the molecular weights of the gases. For comparison, data for a hypothetical *A* labeled nitrogen diffusing into an identical *B* labeled nitrogen is also presented in Figure 5. Here, at steady state, the concentration profile of *A* labeled nitrogen is linear. Reference to Equation (4) written for components *A* and *B* shows that D_{KA} differs from D_{KB} [see Equation (2)], whereas D_{AB} is equal to D_{BA}. Thus, any nonlinearity in the steady state isobaric concentration profile must be attributable to the presence of Knudsen flow. The fact that such nonlinearity exists for methane and for carbon dioxide in Figure 5 supports the conclusion that both Knudsen and bulk diffusion processes were significant

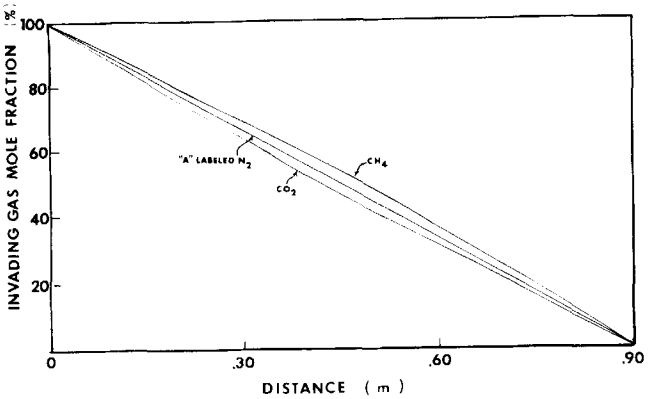

Fig. 5. Analytical results for diffusional flow of methane, carbon dioxide, and labeled nitrogen into nitrogen.

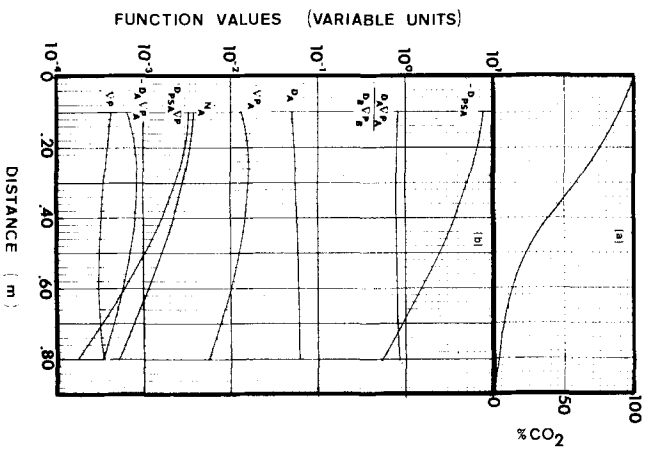

Fig. 6. Flow parameters for combined flow of carbon dioxide into nitrogen.

for the experimental system employing Kaolinite.

In order to document that combined pressure and diffusional flow were treated and to illustrate some characteristics of such a flow system, analytical data were obtained for carbon dioxide flowing into nitrogen under a pressure difference of 3.4×10^3 Pa in Kaolinite. This corresponds to the system shown in Figure 4*f*. The data for $t = 7{,}200$ s (nonsteady state) is shown in Figure 6. The upper curve (Figure 6*a*) shows the concentration profile of carbon dioxide on an arithmetic scale. The S shape of the curve is an indication that both pressure and diffusional processes are operative. Figure 6*b* substantiates this conclusion by presenting other pertinent data extracted from the computer solution and referenced to Equation (18). The product $D_{psA}\nabla P$ represents the pressure related flux of component A, while the product $D_A\nabla p_A$ represents the diffusional flux of component A. It may be seen that the pressure flux dominates at the left end of the tube, whereas the diffusional flux dominates at the right end. Thus, it may be concluded that both Poiseuille and diffusional processes were significant for the experimental system employing Kaolinite.

Two points of analytical interest are also shown in Figure 6*b*. First the diffusion coefficients D_A and, more particularly, D_{psA} are seen to vary considerably with position. A similar variation was noted in time. Thus, approximate approaches to analysis involving constant diffusion coefficients could introduce considerable error. Second, the ratio of the diffusional flux of component A to the diffusional flux of component B is represented in Figure 6*b* by $-D_A\nabla p_A/D_B\nabla p_B$. Much discussion is devoted in the literature to the value of this flux ratio. For isobaric diffusion, this ratio can be shown analytically to be equal to $\sqrt{M_B/M_A}$, facilitating the solution of Equation (14). However, this is not the case for nonsteady state pressure and diffusional flow. Nevertheless, the flux ratio shown in Figure 6*b* varies from 0.811 to 0.846. These values are not greatly different from the square root molecular weight ratio (0.797). It is important to note, however, that this would not likely be the case for higher pressure differences.

NOTATION

A, B = substitutes for i and j in a binary gas system
D_A = diffusion coefficient defined by Equation (18)
D_{ij}^o = bulk diffusion coefficient for gas combination i, j at 1 atm
D_{Ki} = Knudsen diffusion coefficient
D_{psA} = diffusion coefficient defined by Equation (19)
F = total pressure flow flux
$f_v(r)$ = volume fraction of sample composed of pores having radius, r
i, j = gas types
K_i = Knudsen diffusivity
M_i = molecular weight of component i
n = number of gas types in a multicomponent system
N_i = diffusion flux of component i
N_i^P = pressure flux of component i
N_i^T = total flux for component i
N_{Ki} = Knudsen diffusional flux for component i
P = total pressure
$\dot{P}$ = $\partial P/\partial t$ = time rate of change of total pressure
p_i = partial pressure of component i
$\dot{p}_i$ = $\partial p_i/\partial t$ = time rate of change of partial pressure of component i
R = gas constant
r = capillary or pore radius (m)
$r_{\min}$ = smallest pore radius
$r_{\max}$ = largest pore radius
S_{mix} = parameter for slip flow in mixed gas
T = temperature (°K)
t = time
$\overline{v_i}$ = mean thermal velocity of gas i
x_i = mole fraction of gas i
z = spatial coordinate

Greek Letters

Δt = time increment for numerical solution
∇ = operator $\partial/\partial z$
μ_i = viscosity of gas i
μ_{mix} = viscosity of mixed gases
Φ_{ij} = parameter for computing viscosity of mixed gases
τ = tortuosity

LITERATURE CITED

Alzaydi, A. A., "Flow of Gases through Porous Media," Ph. D. dissertation, The Ohio State Univ., Columbus (1975).

Buddenberg, J. W., and C. R. Wilke, "Calculation of Gas Mixture Viscosities," *J. Ind. Eng. Chem.*, **41**, 1345 (1949).

Evans, R. B., G. M. Watson, and E. A. Mason, "I. Gaseous Diffusion in Porous Media, II. Effect of Pressure Gradients," *J. Chem. Physics*, **36**, No. 7, 1394-1902 (1962).

Gunn, R. D., and C. J. King, "Mass Transport in Porous Materials under Combined Gradients of Composition and Pressure," *AIChE J.*, **15**, No. 4, 507-514 (1969).

Knudsen, M., "The Laws of Molecular and Viscous Flow of Gases through Tubes," *Ann. Phys.*, **28**, 75 (1909).

Petersen, E. E., *AIChE J.*, **4**, 343 (1958).

Rai, I. S., and C. A. Moore, "Numerical Solution of Multicomponent Gas Flow," in preparation, (1977).

Remick, R. R., and C. J. Geankoplis, "Binary Diffusion of

Gases in Capillaries in the Transition Region between Knudsen and Molecular Diffusion," *Ind. Eng. Chem. Fundamentals*, 12, 214 (1973).
Rothfeld, L. B., "Gaseous Counterdiffusion in Catalyst Pallets," *AIChE J.*, 9, No. 1, 19-24 (1963).
Satterfield, C. N., and P. J. Cadle, "Diffusion and Flow in Commercial Catalysts at Pressure Levels about Atmospheric," *J. Ind. Eng. Chem. Fundamentals*, 7, 202 (1968).
Scott, D. S., and F. A. L. Dullien, "Diffusion of Ideal Gases in Capillaries and Porous Solids," *AIChE J.*, 8, No. 1, 113-117 (1962).
Wheeler, A., *Catalysis*, Vol. 2, Reinhold, New York (1955).
Wilke, C. R., "A Viscosity Equation for Gas Mixtures," *J. Chem. Phys.*, V. 18, No. 4, pp. 517-519 (1950).
Youngquist, G. R., "Diffusion and Flow of Gases in Porous Solids," in *Flow Through Porous Media*, American Chemical Society Publications (1970).

Manuscript received January 19, 1977; revision received August 18, and accepted August 24, 1977.

Collocation Solution of Creeping Newtonian Flow Through Periodically Constricted Tubes with Piecewise Continuous Wall Profile

MARIANO A. NEIRA
and
A. C. PAYATAKES

Chemical Engineering Department
University of Houston
Houston, Texas 77004

A collocation solution of creeping Newtonian flow through periodically constricted tubes is obtained. The profile of the wall of the type of tube considered is piecewise continuous, composed of symmetric parabolic segments. A transformation of the domain of interest into a rectangular one is obtained, which allows satisfaction of all boundary conditions. The collocation solution gives the stream function in terms of the new independent variables and can easily be converted to the original cylindrical coordinates. Axial and radial velocity components are obtained in analytical form, and the pressure drop is calculated from a volume integration of the viscous dissipation function as well as from line integration of the Navier-Stokes equation. The results are compared with the finite-difference solution by Payatakes et al. (1973*b*) and are found in good agreement. Differences between the two solutions are attributed mainly to discretization error in the finite-difference solution. The analytical expressions obtained from the collocation solution can be used together with porous media models of the constricted unit cell type for the modeling of processes taking place in granular porous media.

SCOPE

The problem of laminar flow through periodically constricted tubes usually arises in connection with porous media modeling. Petersen (1958) used this concept to derive an expression for the effective diffusion coefficient in porous pellets. Houpeurt (1959), independently, considered periodically constricted tubes as building elements in his analysis of flow through porous media. These authors, however, did not propose a method for the determination of the geometry of the periodically constricted tubes from experimental measurements, nor did they solve the associated flow problem.

Payatakes, Tien, and Turian (1973*a*) developed a model for granular porous media which employs unit cells that resemble segments of constricted tubes and the geometry and size distribution of which are determined from simple experimental measurements. They postulated that the flow through a given unit cell is identical to that through a segment of the corresponding periodically constricted tube. The latter problem was solved in Payatakes, Tien, and Turian (1973*b*) using a finite-difference method of the stream function-vorticity type. That method can be applied to periodically constricted tubes with different types of wall geometries, even with discontinuities (see also Payatakes, Tien, and Turian, 1973*c*), and it retains the nonlinear terms of the equation of motion. The porous media model of Payatakes et al. (1973*a, b*) was used as basis for the modeling of liquid filtration in deep granular beds with good results (Payatakes, Tien, and Turian, 1974*a, b*; Payatakes, Brown, and Tien, 1977; Rajagopalan and Tien, 1976).

Payatakes and Neira (1977) developed a generalized version of the Payatakes et al. (1973*a*) model by including the random orientation of the unit cells and superimposing a random network structure which accounts for the pore interconnectivity.

Slattery (1974) and Oh and Slattery (1976) used periodically constricted tubes in the analysis of the forces acting on oil ganglia during tertiary oil recovery by flooding in

0001-1541/78/9195-0043/$01.35